Journal of Solid State Chemistry 183 (2010) 1985–1991

Contents lists available at ScienceDirect

Journal of Solid State Chemistry

journal homepage: www.elsevier.com/locate/jssc

The ionic conductivity and local environment of cations in Bi_9ReO_{17}

M. Thompson [a], T. Herranz [b], B. Santos [b], J.F. Marco [b], F.J. Berry [a], C. Greaves [a,*]

[a] School of Chemistry, University of Birmingham, Edgbaston, Birmingham B15 2TT, UK
[b] Instituto de Quimica-Fisica "Rocasolano", Consejo Superior de Investigaciones Cientificas, Serrano 119, 28006 Madrid, Spain

ARTICLE INFO

Article history:
Received 4 May 2010
Received in revised form
28 June 2010
Accepted 28 June 2010
Available online 16 July 2010

Keywords:
Bi_9ReO_{17}
Bismuth rhenium oxide
Neutron diffraction
Oxide ion conductivity

ABSTRACT

The influence of temperature on the structure of Bi_9ReO_{17} has been investigated using differential thermal analysis, variable temperature X-ray diffraction and neutron powder diffraction. The material undergoes an order–disorder transition at ~1000 K on heating, to form a fluorite-related phase. The local environments of the cations in fully ordered Bi_9ReO_{17} have been investigated by Bi L_{III}- and Re L_{III}-edge extended X-ray absorption fine structure (EXAFS) measurements to complement the neutron powder diffraction information. Whereas rhenium displays regular tetrahedral coordination, all bismuth sites show coordination geometries which reflect the importance of a stereochemically active lone pair of electrons. Because of the wide range of Bi–O distances, EXAFS data are similar to those observed for disordered structures, and are dominated by the shorter Bi–O bonds. Ionic conductivity measurements indicate that ordered Bi_9ReO_{17} exhibits reasonably high oxide ion conductivity, corresponding to $2.9\times10^{-5}\,\Omega^{-1}\,cm^{-1}$ at 673 K, whereas the disordered form shows higher oxide ion conductivity ($9.1\times10^{-4}\,\Omega^{-1}\,cm^{-1}$ at 673 K).

1. Introduction

The δ-form of bismuth oxide, Bi_2O_3, is observed as the high temperature cubic phase at temperatures exceeding 1003 K. The δ-Bi_2O_3 phase adopts an anion-deficient fluorite-related structure in which 25% of the anion sites are vacant [1,2]. These disordered anion vacancies induce an oxide ion conductivity [3] which is two to three orders of magnitude greater than those observed in calcium- or yttrium-stabilised zirconia [4]. The δ-Bi_2O_3 structure can be retained at room temperature by doping with ca. 15–42 mol% of iso- or alio-valent cations [3–11]—however, at least over short distances, the dopants appear to induce ordering of the anion vacancies and a consequent reduction in oxide ion conduction.

The substitution of small amounts of bismuth by metal oxoanions in Bi_2O_3 has been shown to produce stable structures with some displaying relatively high oxide ion conductivity. For example, $Bi_{28}Re_2O_{49}$ adopts a superstructure of the cubic fluorite unit cell, with both octahedral ReO_6^{5-} and tetrahedral ReO_4^- units, and comprises an ordered framework of linked BiO_4 trigonal bipyramids and square pyramids with discrete rhenium oxoanions at the origin and body centre of the unit cell [12]. Despite its ordered structural framework, the compound displays relatively high oxide ion conductivity ($5.4\times10^{-4}\,\Omega^{-1}\,cm^{-1}$ at 673 K), within an order of magnitude of the conductivity observed for the Y-stabilised δ-Bi_2O_3 phase $(Bi_{0.75}Y_{0.25})_2O_3$.

As a development of that work we have initiated further studies of the structural and conduction properties of other fluorite-related superstructures in the bismuth-rich portion of the Bi_2O_3–Re_2O_7 phase diagram, including the material of composition Bi_9ReO_{17} which, when formed by quenching from high temperature, has been suggested [13] to contain both ReO_4 and ReO_6 environments, similar to those observed in $Bi_{28}Re_2O_{49}$, although the actual ordered structure of the slow cooled material was not known at that time. However, during the course of our studies the structure of Bi_9ReO_{17} was described [14]. Here we report a complementary structural study of Bi_9ReO_{17} by X-ray (XRD) and neutron powder diffraction (NPD) together with the results of an examination of the local environments of the cations by extended X-ray absorption spectroscopy (EXAFS) and its oxide ion conduction properties. The structural description is slightly different from that previously given [14] and emphasises the preferred stereochemical preference of Bi^{3+}.

2. Experimental

The material of composition Bi_9ReO_{17} was prepared from stoichiometric amounts of the high purity reagents Bi_2O_3 (Aldrich, 99.9%) and NH_4ReO_4 (Aldrich, 99+%) which were intimately ground and calcined in air at 1073 K for 12 h. Several cycles of regrinding and reheating were performed until a single phase product was obtained.

XRD patterns were recorded in transmission mode with a Siemens D5000 and a Bruker D8 diffractometer, both using a germanium primary beam monochromator and Cu$K\alpha_1$ radiation

* Corresponding author.
E-mail address: c.greaves@bham.ac.uk (C. Greaves).

0022-4596/$ - see front matter © 2010 Elsevier Inc. All rights reserved.
doi:10.1016/j.jssc.2010.06.017

of wavelength 1.5406 Å. Variable temperature data were collected on a Bruker D8 diffractometer operating in reflection mode. Differential thermal analysis (DTA) information was collected from a Netzsch STA 449C Jupiter instrument.

EXAFS measurements were performed in transmission mode at The European Synchrotron Radiation Facility ESRF in Grenoble, France on Beamline 25 at 298 K. The raw data were background subtracted and normalised using the programme ATHENA [15]. The EXAFS oscillations were isolated from the raw data, weighted by k^2 and fitted using the software package ARTEMIS [15].

NPD measurements were performed on the super-D2B diffractometer at ILL, Grenoble. A wavelength of 1.594 Å was used with the sample (~5 g) contained in a vanadium can of 8 mm diameter.

The oxide ion conductivity was recorded from pellets formed by pressing the powdered sample in a pellet press using an 8 mm diameter die and a pressure of ~1.5 tonne cm^{-2}. Pellets were sintered at a temperature of 1123 K for 16 h with a heating and cooling rate of 60 K/h for Bi_9ReO_{17}, whereas the high temperature face-centred cubic form of Bi_9ReO_{17} was retained at room temperature by quenching a pellet from 1123 K into liquid nitrogen; pellet densities were 85–90% of the theoretical value. Contact between the face of the pellet and the electrodes was achieved by the use of silver paste, and conductivity measurements were made using a Solartron SI 1260 Impedance Analyser over the temperature range 473–923 K and the frequency range 1 Hz–1×10^6 Hz in air.

3. Results and discussion

Neutron powder diffraction data were recorded from Bi_9ReO_{17} at 3 and 300 K, and refinement was based upon a structure with monoclinic symmetry, space group $P2_1/c$ [14]. The low temperature data were recorded to provide better statistical precision, as it was envisaged that the reduction in thermal parameters would be useful for reducing thermal effects in the subsequent structure determination/refinement. Emphasis is therefore placed on the results from this dataset. The resultant unit cell parameters (a=9.87892(8), b=19.6100(2), c=11.5926(1) Å, β=125.2967(4)° at 3 K and a=9.9030(2), b=19.7139(4), c=11.6212(2) Å, β=125.2988(7)° at 300 K) are consistent with the previous ambient temperature refinement [14], where a=9.89917(5), b=19.70356(10), c=11.61597(6) Å, β=125.302(2)°. Refinement statistics for 159 variables were R_p=0.0222, wR_p=0.0287 and χ^2=2.772 for the data recorded at 3 K, and R_p=0.0281, wR_p=0.0359 and χ^2=1.698 for the data recorded at 300 K. The refined structural information is shown in Table 1, and fitted NPD profiles for the data recorded at 3 K shown in Fig. 1, which shows good agreement between observed and calculated profiles. The data are of high quality and no constraints on temperature factors are required. Whereas all refined temperature factors (Table 1) were reasonable for the 3 K dataset ($0.18\ Å^2 \le 100U_{iso} \le 1.0\ Å^2$), some high values were obtained for the 300 K data, as was found previously [14]. In particular, the O atoms forming the ReO_4^- tetrahedra (O1, O2, O3, O4) have a significantly enhanced U_{iso} at 300 K (average 2.65 $Å^2$) compared with the other O atoms which are bonded only to Bi (average 1.79 $Å^2$). This is probably related to librational dynamics of the ReO_4 groups, and is consistent with thermal analysis and conductivity data (*vide infra*).

Metal–oxygen distances in Bi_9ReO_{17} at both 3 and 300 K are given in Table 2, and allow comparison with the full range of distances provided in the earlier determination [14]. It can be seen that many of the Bi–O distances are very long, and are substantially larger than those which are normally ascribed to

Table 1
Refined structural parameters for Bi_9ReO_{17} at 3 and 300 K.

Atom	Multiplicity	3 K a=9.87892(8), b=19.6100(2), c=11.5926(1) Å, β=125.2967(4)°				300 K a=9.9030(2), b=19.7139(4), c=11.6212(2) Å, β=125.2988(7)°			
		x	y	z	$U_{iso} \times 100$ (Å^2)	x	y	z	$U_{iso} \times 100$ (Å^2)
Re	4	0.6342(4)	0.4394(2)	0.1799(3)	0.18(8)	0.6326(6)	0.4389(3)	0.1805(5)	1.1(1)
Bi1	4	0.0841(2)	0.2535(2)	0.4041(4)	0.56(9)	0.0830(8)	0.2537(4)	0.4025(7)	1.4(2)
Bi2	4	0.6061(5)	0.2734(2)	0.6839(4)	0.52(7)	0.6098(8)	0.2728(3)	0.6858(7)	1.4(1)
Bi3	4	0.1060(4)	0.0530(3)	0.4396(3)	0.27(8)	0.1033(7)	0.0514(4)	0.4357(5)	1.3(1)
Bi4	4	0.1355(4)	0.4473(2)	0.4406(4)	0.43(7)	0.1381(6)	0.4477(4)	0.4412(5)	0.9(1)
Bi5	4	0.6184(4)	0.4522(2)	0.6769(4)	0.24(8)	0.6223(7)	0.4516(4)	0.6778(6)	1.1(1)
Bi6	4	0.0848(5)	0.6461(2)	0.3924(4)	0.25(8)	0.0838(8)	0.6475(3)	0.3929(7)	1.2(1)
Bi7	4	0.1104(5)	0.8458(2)	0.4466(4)	0.34(8)	0.1115(8)	0.8455(4)	0.4479(7)	1.2(1)
Bi8	4	0.6612(4)	0.8441(2)	0.1943(4)	0.37(7)	0.6612(7)	0.8440(3)	0.1949(6)	1.2(1)
Bi9	4	0.6239(5)	0.6649(2)	0.1881(4)	0.25(8)	0.6216(9)	0.6656(3)	0.1891(7)	1.1(1)
O1	4	0.4565(6)	0.1061(3)	0.6240(6)	0.9(1)	0.454(1)	0.1060(6)	0.625(1)	3.8(3)
O2	4	0.6413(6)	0.4556(3)	0.0365(5)	0.7(1)	0.641(1)	0.4537(5)	0.0393(9)	2.1(2)
O3	4	0.3599(7)	0.4861(3)	0.7416(6)	0.8(1)	0.360(1)	0.4874(5)	0.743(1)	0.8(1)
O4	4	0.1965(7)	0.8895(3)	0.1981(6)	1.0(1)	0.202(1)	0.8901(6)	0.201(1)	3.9(3)
O5	4	0.4482(6)	0.2425(3)	0.7600(6)	0.6(1)	0.446(1)	0.2426(5)	0.760(1)	1.9(1)
O6	4	0.9096(6)	0.2495(3)	0.1705(6)	0.3(1)	0.911(1)	0.2493(5)	0.171(1)	1.6(2)
O7	4	0.5205(7)	0.3630(3)	0.7222(6)	0.8(1)	0.523(1)	0.3628(5)	0.727(1)	1.9(2)
O8	4	0.6739(7)	0.1313(3)	0.0999(6)	0.6(1)	0.673(1)	0.133(5)	0.097(1)	1.6(2)
O9	4	0.3113(7)	0.2419(3)	0.9000(6)	0.5(1)	0.312(1)	0.2415(5)	0.900(1)	1.5(2)
O10	4	0.8291(6)	0.2729(3)	0.8887(5)	0.6(1)	0.830(1)	0.2731(5)	0.8887(9)	1.2(2)
O11	4	0.8904(7)	0.4386(3)	0.9280(6)	0.9(1)	0.890(1)	0.4377(6)	0.931(1)	2.5(2)
O12	4	0.3688(7)	0.0323(2)	0.9823(6)	0.6(1)	0.370(1)	0.0335(4)	0.9839(9)	1.7(2)
O13	4	0.0853(7)	0.3520(3)	0.8324(6)	0.8(1)	0.083(1)	0.3530(5)	0.831(1)	1.9(2)
O14	4	0.1522(6)	0.1573(3)	0.1177(5)	0.5(1)	0.152(1)	0.1570(5)	0.116(1)	1.8(2)
O15	4	0.1082(7)	0.1305(3)	0.8105(6)	0.8(1)	0.107(1)	0.1302(5)	0.811(1)	1.5(2)
O16	4	0.1277(6)	0.3345(3)	0.0929(5)	0.3(1)	0.127(1)	0.3349(5)	0.0926(9)	1.3(2)
O17	4	0.0297(7)	0.9759(3)	0.7791(6)	1.0(1)	0.035(1)	0.9759(5)	0.779(1)	2.9(2)

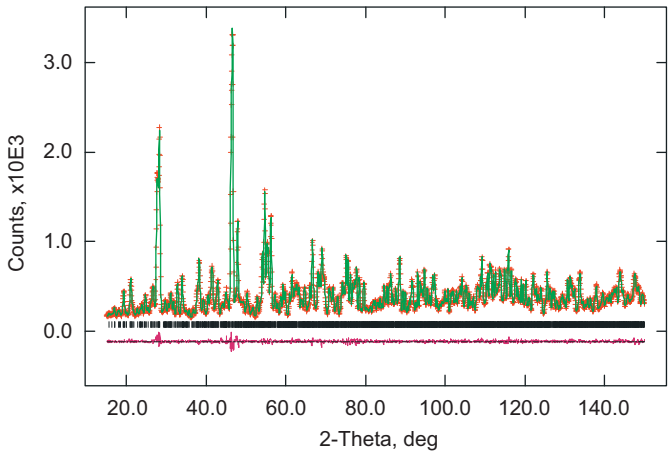

Fig. 1. The observed (+), calculated (−) and difference NPD profiles for the final Rietveld refinement of Bi_9ReO_{17} at 3 K.

Table 2
Selected metal–oxygen distances (Å) in Bi_9ReO_{17} at 3 and 300 K.

Atom 1	Atom 2	3 K	300 K	Atom 1	Atom 2	3 K	300 K
Bi1	O4[a]	3.522(7)	3.57(1)	Bi5	O17	3.242(7)	3.17(1)
Bi1	O6	2.217(7)	2.20(1)	Bi6	O4[a]	3.121(7)	3.14(1)
Bi1	O9	2.275(7)	2.29(1)	Bi6	O6	2.165(7)	2.15(1)
Bi1	O10	2.475(7)	2.47(1)	Bi6	O8	2.352(7)	2.36(1)
Bi1	O13	2.233(7)	2.26(1)	Bi6	O10	3.294(6)	3.29(1)
Bi1	O14	2.777(7)	2.78(1)	Bi6	O13	2.135(7)	2.13(1)
Bi1	O15	2.589(8)	2.59(1)	Bi6	O14	2.287(6)	2.28(1)
Bi1	O16	2.621(7)	2.65(1)	Bi6	O17	2.631(7)	2.68(1)
Bi2	O1[a]	3.501(7)	3.52(1)	Bi7	O2[a]	3.184(6)	3.19(1)
Bi2	O4[a]	3.578(6)	3.56(1)	Bi7	O4[a]	3.549(7)	3.58(1)
Bi2	O5	2.274(7)	2.30(1)	Bi7	O6	2.268(7)	2.28(1)
Bi2	O6	3.123(6)	3.11(1)	Bi7	O7	3.460(6)	3.42(1)
Bi2	O7	2.105(7)	2.14(1)	Bi7	O10	2.174(7)	2.17(1)
Bi2	O8	2.374(7)	2.38(1)	Bi7	O11	2.332(7)	2.31(1)
Bi2	O9	2.885(7)	2.91(1)	Bi7	O15	2.515(7)	2.54(1)
Bi2	O10	2.109(6)	2.09(1)	Bi7	O16	2.132(6)	2.14(1)
Bi3	O1[a]	3.015(6)	3.04(1)	Bi8	O1[a]	3.095(6)	3.07(1)
Bi3	O2[a]	3.026(7)	3.06(1)	Bi8	O5	2.235(6)	2.23(1)
Bi3	O11	2.707(7)	2.71(1)	Bi8	O8	3.127(7)	3.12(1)
Bi3	O11	2.062(6)	2.09(1)	Bi8	O9	2.111(7)	2.12(1)
Bi3	O13	2.183(7)	2.19(1)	Bi8	O12	3.074(6)	3.08(1)
Bi3	O16	2.763(7)	2.81(1)	Bi8	O15	2.364(6)	2.39(1)
Bi3	O17	2.149(7)	2.11(1)	Bi8	O16	2.127(6)	2.13(1)
Bi4	O3[a]	2.954(7)	2.97(1)	Bi9	O1[a]	3.426(7)	3.48(1)
Bi4	O4[a]	2.922(7)	2.99(1)	Bi9	O2[a]	3.369(6)	3.37(1)
Bi4	O7	3.676(7)	3.70(1)	Bi9	O3[a]	3.051(6)	3.10(1)
Bi4	O12	2.102(6)	2.08(1)	Bi9	O5	2.159(7)	2.13(1)
Bi4	O14	2.839(7)	2.84(1)	Bi9	O7	2.265(7)	2.22(1)
Bi4	O15	2.050(7)	2.05(1)	Bi9	O9	2.356(7)	2.38(1)
Bi4	O17	2.147(7)	2.15(1)	Bi9	O13	3.035(7)	3.09(1)
Bi5	O3[a]	3.120(7)	3.17(1)	Bi9	O14	2.057(6)	2.08(1)
Bi5	O7	2.205(6)	2.24(1)	Re	O1	1.726(6)	1.73(1)
Bi5	O8	2.085(7)	2.11(1)	Re	O2	1.735(5)	1.714(9)
Bi5	O11	2.594(6)	2.59(1)	Re	O3	1.705(6)	1.69(1)
Bi5	O12	2.482(6)	2.51(1)	Re	O4	1.738(6)	1.70(1)
Bi5	O12	2.198(6)	2.21(1)				

[a] O atoms bonded to Re.

strong bonds. In fact, no significant discussion of the bismuth stereochemistry was provided in the previous structure determination [14]. It can be seen that for each Bi site, there are three or four short Bi–O distances, and Table 3 provides an evaluation based on a maximum bond distance of 2.4 Å for the 3 K data. The table also shows the individual bismuth coordination polyhedra and selected bond angles for each Bi and Re atom. Re is present as almost undistorted ReO_4 tetrahedra with an average Re–O bond of 1.726 Å. The bond distance criterion assumed provides two distinctly different coordination environments for the Bi sites, both of which are fully consistent with those expected for ions with a stereochemically active lone pair (e) such as Bi^{3+}. Bi1, Bi3, Bi4 and Bi5 are three-coordinate with pyramidal coordination (tetrahedral including the lone pair, BiO_3e) and O–Bi–O angles all substantially less than the tetrahedral angle, which is consistent with significant lone pair–bond pair electron repulsions. The remaining Bi sites (Bi2, Bi6, Bi7, Bi8, Bi9) are four-coordinate with pseudo-trigonal bipyramidal coordination including an equatorial lone pair of electrons (BiO_4e). In all cases, Table 3 shows that the axial bonds, with largest O–Bi–O angle, are slightly longer than the equatorial bonds; this is in accordance with simple electron-pair repulsion theory and conforms with higher bond pair–lone pair electron repulsions for these bonds which are at 90° to the lone pair direction in the ideal undistorted trigonal bipyramid stereochemistry.

Bond valence sum (BVS) calculations [16] for the cation sites (Table 3) reveal that the stereochemistries described completely satisfy the Bi^{3+} bonding requirements for the four-coordinate sites but are somewhat lower for the pyramidal sites. Bi1 is notably low at 2.02, and for this site, significant contributions to the bonding will be provided by slightly more distant O atoms. Indeed, Table 2 shows that at this position O10, O15 and O16 atoms are quite close to Bi1, and including these in the calculations provides a BVS of 2.88. The Re BVS is high (7.74) but still only ~10% different from that expected [16].

The average Re–O bond distance (1.726 Å) is consistent with those previously reported in bismuth rhenium oxides [12,17]. The Bi–O bonds and directional properties are all consistent with the short Bi–O bonds in other bismuth and bismuth rhenium oxides. In α-Bi_2O_3 [18] and Bi_3ReO_8 [17] for example, there are three short Bi–O bonds in a pyramidal arrangement. $Bi_{28}Re_2O_{49}$ [12] is described as having four coordinate BiO_4e sites with both trigonal bipyramidal and square pyramidal configurations.

Fig. 2 shows the structure of Bi_9ReO_{17} based on the stereochemistries described in Table 3: ReO_4 tetrahedra are displayed as polyhedra, and the stereochemical preference of each Bi atom is displayed. A Bi–O network is established which encapsulates isolated tetrahedral ReO_4 units.

The Bi L_{III} edge EXAFS recorded from Bi_9ReO_{17} and the corresponding Fourier transform is shown in Fig. 3. The best fit parameters to the data are given in Table 4. The Bi L_{III} edge EXAFS were not amenable to fitting beyond a first shell coordination of 2.04 oxygen atoms at a distance of 2.14 Å. At first sight, this result therefore appears to provide little support for the NPD data, for which the minimum coordination number is three. However, the Bi–O distance is quite similar to the average of all Bi–O distances less than 2.40 Å (Table 3), which is 2.20 Å, and the corresponding average coordination number is 3.6. The results are similar to those recorded from $Bi_{12.5}Er_{1.5}ReO_{24.5}$ [19] where bismuth was fitted to a first shell coordination of 1.84 oxygen atoms at a distance of 2.12 Å. $Bi_{12.5}Er_{1.5}ReO_{24.5}$ is highly disordered, with a wide range of Bi–O distances [20], and this was assumed to result in the EXAFS data being dominated by the shorter Bi–O distances. We believe a similar situation can explain the present results, even though we are now exploring a fully ordered structure. The nine individual Bi sites all have a different range of Bi–O distances, making the situation similar to that relating to a highly disordered system. The EXAFS data are therefore weighted in favour of the shorter bond distances. Indeed, using only the shorter Bi–O NPD distances – those from the three bonds of the pyramidal sites and the equatorial positions of the trigonal bipyramidal sites – we obtain an average Bi–O distance of 2.14 Å, and an average coordination of 2.4. These data are seen to be in good agreement with the EXAFS results and add support to the high sensitivity of the EXAFS data to the shorter distances.

Table 3
Selected metal–oxygen distances up to 2.4 Å (3 K data), along with coordination polyhedra and bond angles. Some O atoms are labelled for clarity.

Bond lengths (Å)			Stereochemistry	Bond angles (deg)		BVS
Bi1	O6	2.217(7)	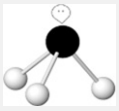	O6–Bi1–O9	93.2(2)	2.02
	O9	2.275(7)		O6–Bi1–O13	71.3(2)	
	O13	2.233(7)		O9–Bi1–O13	79.1(3)	
Bi2	O5	2.274(7)	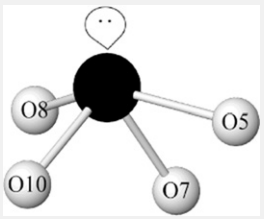	O5–Bi2–O7	72.0(2)	3.01
	O7	2.105(7)		O5–Bi2–O8	142.0(3)	
	O8	2.374(7)		O5–Bi2–O10	93.8(3)	
	O10	2.109(6)		O7–Bi2–O8	70.9(2)	
				O7–Bi2–O10	93.0(3)	
				O8–Bi2–O10	96.1(3)	
Bi3	O11	2.062(6)	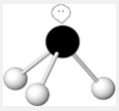	O11–Bi3–O13	98.2(3)	2.74
	O13	2.183(7)		O11–Bi3–O17	91.5(3)	
	O17	2.149(7)		O13–Bi3–O17	76.4(2)	
Bi4	O12	2.102(6)	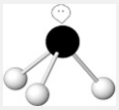	O12–Bi4–O15	88.4(3)	2.97
	O15	2.050(7)		O12–Bi4–O17	89.1(3)	
	O17	2.147(7)		O15–Bi4–O17	95.1(3)	
Bi5	O7	2.205(6)	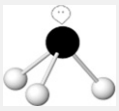	O7–Bi5–O8	74.8(3)	2.52
	O8	2.085(7)		O7–Bi5–O12	88.1(3)	
	O12	2.198(6)		O8–Bi5–O12	92.3(2)	
Bi6	O6	2.165(7)	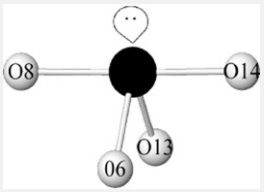	O6–Bi6–O8	84.6(2)	2.81
	O8	2.352(7)		O6–Bi6–O13	74.2(2)	
	O13	2.135(7)		O6–Bi6–O14	96.8(3)	
	O14	2.287(6)		O8–Bi6–O14	178.3(3)	
				O13–Bi6–O14	82.8(3)	
Bi7	O6	2.268(7)	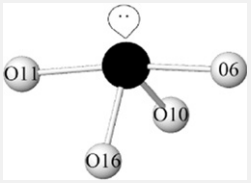	O6–Bi7–O10	82.1(3)	2.86
	O10	2.174(7)		O6–Bi7–O11	173.2(3)	
	O11	2.332(7)		O6–Bi7–O16	94.6(3)	
	O16	2.132(6)		O10–Bi7–O11	93.7(2)	
				O10–Bi7–O16	80.2(2)	
				O11–Bi7–O16	79.3(3)	
Bi8	O5	2.235(6)	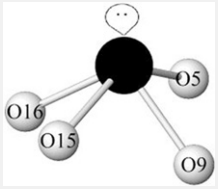	O5–Bi8–O9	74.9(2)	3.04
	O9	2.111(7)		O5–Bi8–O15	140.4(3)	
	O15	2.364(6)		O5–Bi8–O16	86.7(2)	
	O16	2.127(6)		O9–Bi8–O15	75.1(2)	
				O9–Bi8–O16	101.3(3)	
				O15–Bi8–O16	74.5(2)	
Bi9	O5	2.159(7)	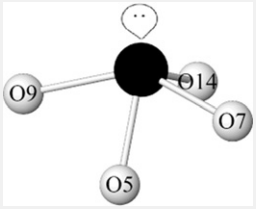	O5–Bi9–O7	71.2(2)	3.07
	O7	2.265(7)		O5–Bi9–O9	71.6(2)	
	O9	2.356(7)		O5–Bi9–O14	94.3(2)	
	O14	2.057(6)		O7–Bi9–O9	142.0(3)	
				O7–Bi9–O14	92.5(2)	
				O9–Bi9–O14	98.1(3)	
Re	O1	1.726(6)	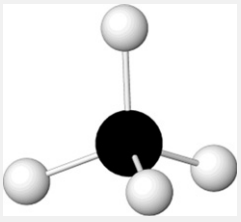	O1–Re1–O2	109.3(3)	7.74
	O2	1.735(5)		O1–Re1–O3	110.9(3)	
	O3	1.705(6)		O1–Re1–O4	107.9(3)	
	O4	1.738(6)		O2–Re1–O3	110.3(3)	
				O2–Re1–O4	109.3(3)	
				O3–Re1–O4	109.1(3)	

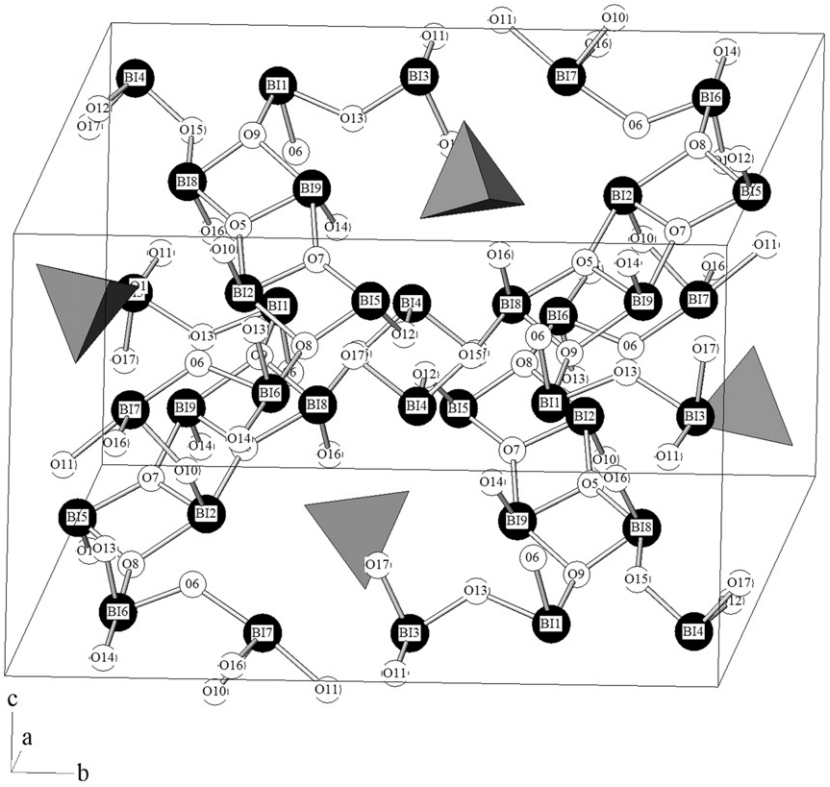

Fig. 2. The structure of Bi_9ReO_{17}, where the black atoms represent Bi, white represent O and ReO_4 tetrahedra are shown in grey.

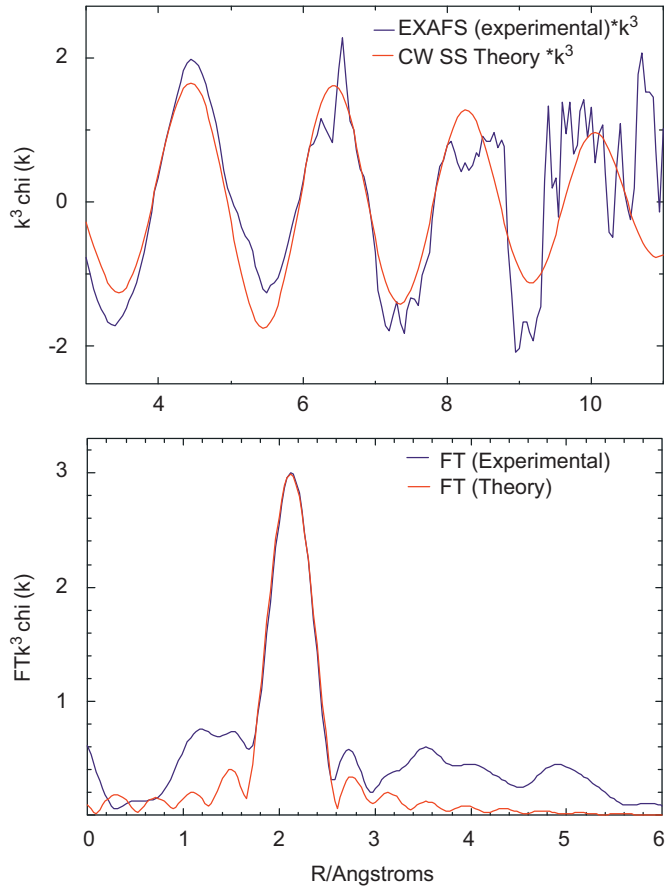

Fig. 3. The Bi L_{III} edge EXAFS of Bi_9ReO_{17} and corresponding Fourier transform.

Table 4
Best-fit parameters to the Bi L_{III} and Re L_{III} edge EXAFS recorded from Bi_9ReO_{17}.

Edge	Coordination number	Bond distance±0.03 (Å)	$2\sigma^2$ (Å^2)
Bi L3	2.04	2.14	0.005
Re L3	4	1.74	0.001

The Re L_{III} edge EXAFS recorded from Bi_9ReO_{17} and the corresponding Fourier transform is shown in Fig. 4. The best fit parameters are given in Table 4. The data were fitted to a first shell coordination of four oxygen atoms at a distance of 1.74 Å, in excellent agreement with the NPD refinement results (Table 3) and similar to the Re L_{III} edge EXAFS recorded from $Bi_{12.5}Er_{1.5}ReO_{24.5}$ [19], where rhenium is tetrahedrally coordinated to oxygen at 1.76 Å. Attempts to refine the first shell of the Re L_{III} edge EXAFS to six fold oxygen coordination gave unsatisfactory fits to the data, confirming the NPD results that rhenium exists only in tetrahedral coordination to oxygen in contrast to the local environment in $Bi_{28}ReO_{49}$ [12], which contains both octahedrally and tetrahedrally coordinated rhenium. As for the Bi L_{III} edge EXAFS data, the Re L_{III} edge EXAFS could not be fitted beyond a first shell. The small Debye–Waller factor for the rhenium coordination is consistent with the presence of rhenium in well defined, discrete ReO_4 tetrahedra.

DTA information (Fig. 5) showed an endothermic transition (onset ~1000 K) on heating. Marked hysteresis occurs, and the corresponding transition on cooling is seen with an onset at ~940 K. Variable temperature XRD data (Fig. 6) show that the thermal effects relate to a structural transition to give an fcc fluorite-related structure in the high temperature regime. The trace at a nominal temperature of 1020 K shows peaks corresponding to both low temperature (monoclinic) and high

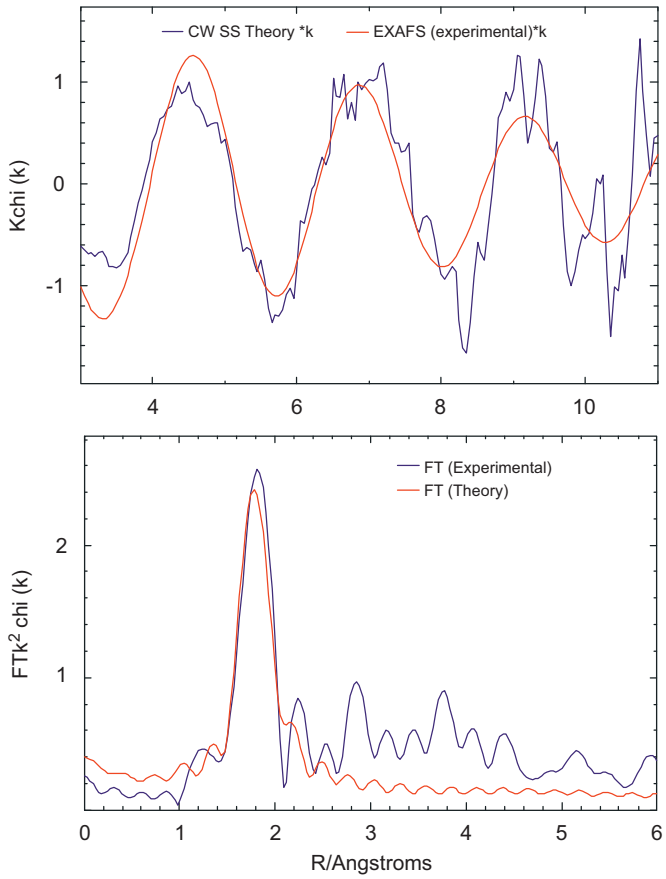

Fig. 4. The Re L_{III} edge EXAFS of Bi_9ReO_{17} and corresponding Fourier transform.

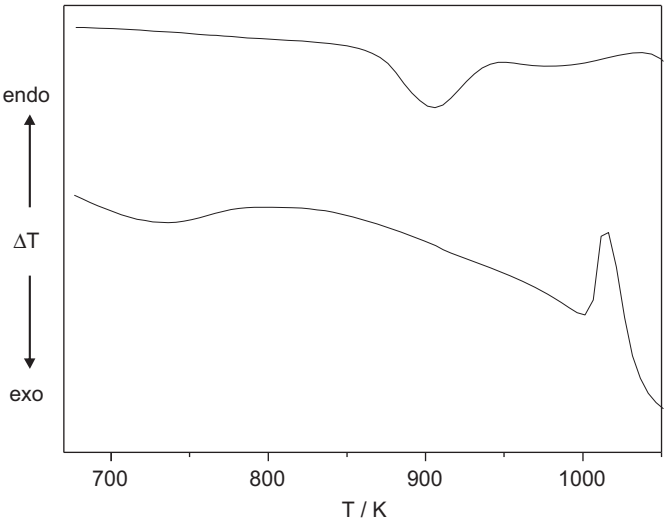

Fig. 5. DTA plots for Bi_9ReO_{17}, showing heating curve (lower) and cooling curve (upper).

temperature (cubic) forms. It was found that the high temperature, disordered, fcc form could be retained at ambient temperature by quenching pellets from 1123 K into liquid nitrogen.

Impedance spectroscopy was used to collect oxide ion conductivity data over the temperature range 473–923 K for Bi_9ReO_{17}, and 473–673 K for the fcc quenched form of Bi_9ReO_{17}. Extended periods at temperatures above 673 K resulted in the cubic structure transforming into a new structure, as yet incompletely characterised. XRD data confirmed that both the monoclinic and cubic phases had retained their structures throughout the impedance measurements. The complex plane impedance plots could be fitted to a single semicircle (Fig. 7) and resistance was therefore assigned to bulk effects; electronic contributions to conductivity were assumed to be negligible as previously found for similar bismuth rhenium oxides [20]. The conductivity was determined from the extrapolated intercept of the semicircle with the real axis in the complex plane plots. Fig. 8 shows the plots of log σ versus 1000 K/T for Bi_9ReO_{17} and the high temperature cubic form of Bi_9ReO_{17}. As expected, the disordered fcc structure provides enhanced conductivity, with an Arrhenius activation energy, E_a, of 0.69 eV. The fully ordered Bi_9ReO_{17} displayed good oxide ion conductivity of $2.9\times10^{-5}\,\Omega^{-1}\,cm^{-1}$ at 673 K, but significantly lower than that of $Bi_{28}Re_2O_{49}$ at the same temperature, $5.4\times10^{-4}\,\Omega^{-1}\,cm^{-1}$ [12]. This is consistent with the suggestion [3] that in doped bismuth oxide materials the conductivities decrease with increasing substituent oxide content, but may also indicate that the two different coordinations for Re in $Bi_{28}Re_2O_{49}$ (octahedral and tetrahedral) may be involved in its conduction mechanism as previously suggested [12]. Although the plot for slow cooled Bi_9ReO_{17} is linear below ~690 K, with E_a=0.99 eV, an upturn in

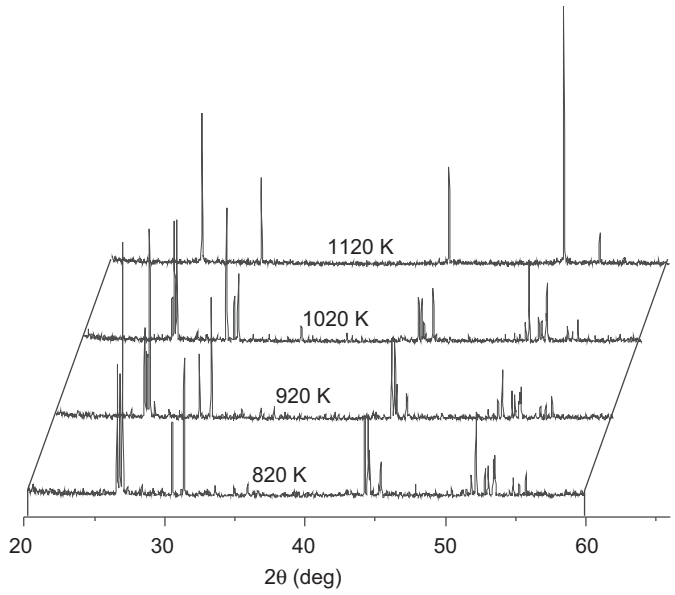

Fig. 6. Variable temperature XRD patterns showing the transition to an fcc fluorite-related structure at elevated temperatures.

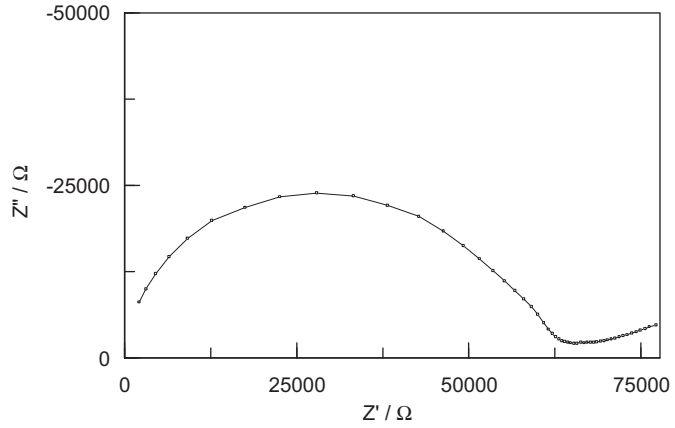

Fig. 7. Complex plane plot for quenched Bi_9ReO_{17} at 370 K.

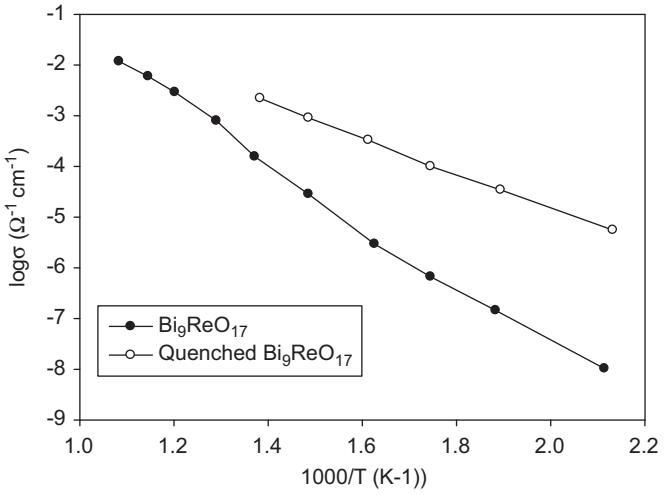

Fig. 8. Arrhenius plots of conductivity determined by impedance spectroscopy for ordered and quenched Bi_9ReO_{17}.

conductivity is seen at higher temperatures. This upturn could relate to enhanced libration/rotation of the ReO_4 groups within the otherwise ordered Bi_9ReO_{17} structure, and the onset correlates quite well with the onset ($\sim$720 K) of what could be a very broad endotherm in the DTA trace (Fig. 5). The conductivity recorded for Bi_9ReO_{17} at 773 K, $8.0\times10^{-4}\,\Omega^{-1}\,cm^{-1}$, is similar to that observed for other well characterised stabilised bismuth oxide ion conductors, and is just outside an order of magnitude of the fcc ionic conductor $(Bi_2O_3)_{0.8}(Ta_2O_5)_{0.2}$ which has a conductivity of $5.0\times10^{-3}\,\Omega^{-1}\,cm^{-1}$ at 773 K [3].

The high temperature face-centred cubic form of Bi_9ReO_{17} shows improved oxide ion conductivity, as expected for this disordered δ-Bi_2O_3 structure. This high level of anion disorder is undoubtedly responsible for the much improved conductivity in this material with identical composition. The difference in activation energy between the disordered and ordered forms of Bi_9ReO_{17} confirms that different conductivity mechanisms apply. The high temperature quenched form of Bi_9ReO_{17} displays a conductivity of $9.1\times10^{-4}\,\Omega^{-1}\,cm^{-1}$ at 673 K, which is greater than that displayed by $Bi_{28}Re_2O_{49}$ at the same temperature ($5.4\times10^{-4}\,\Omega^{-1}\,cm^{-1}$) [12] in accordance with its disordered structure.

4. Conclusions

The structure of Bi_9ReO_{17} previously reported has been confirmed using NPD and EXAFS data, with Re being present as Re(VII) in regular tetrahedral coordination. However, the local bismuth coordination has been reappraised in this study and a model presented which more fully reflects the importance of a stereochemically active $6s^2$ lone pair of electrons on all Bi atoms. Four of the nine bismuth sites are best described as pyramidal BiO_3e, whereas the other five are trigonal bipyramidal BiO_4e. EXAFS data are consistent with this analysis, but demonstrate that the data are dominated by the shorter Bi–O distances. Both the ordered and disordered forms of Bi_9ReO_{17} display relatively high oxide ion conductivity, with that of the disordered structure being 1–2 orders of magnitude higher over the temperature range $473\ K < T < 673\ K$.

Acknowledgments

We acknowledge the European Synchrotron Radiation Facility and thank Dr. G. Castro for assistance in using Beamline 25. We thank The Spanish Ministry of Science and Innovation for Travel Grants (JFM, TH, BS). We also thank EPSRC for financial support and the provision of neutron diffraction facilities. We are grateful to Emma Suard for assistance with the collection of neutron diffraction data. The diffractometers used in this research were obtained/upgraded through the Science City Advanced Materials project: "Creating and Characterising Next Generation Advanced Materials", with support from Advantage West Midlands (AWM) and part funded by the European Regional Development Fund (ERDF).

References

[1] H.A.Z. Harwig, Z. Anorg. Allg. Chem. 444 (1978) 151.
[2] P.D. Battle, C.R.A. Catlow, J. Drennan, A.D. Murray, J. Phys. C 16 (1983) 156.
[3] T. Takahashi, H. Iwahara, Mater. Res. Bull. 13 (1978) 1447.
[4] D.W. Strickler, W.G. Carlson, J. Am. Ceram. Soc. 47 (1964) 12.
[5] N. Jiang, E.D. Wachsman, J. Am. Ceram. Soc. 82 (1999) 3057.
[6] T. Takahashi, H. Iwahara, T. Arao, J. Appl. Electrochem. 5 (1975) 187.
[7] T. Takahashi, T. Esaka, H. Iwahara, J. Appl. Electrochem. 6 (1976) 197.
[8] T. Takahashi, T. Esaka, H. Iwahara, J. Appl. Electrochem. 7 (1977) 299.
[9] T. Takahashi, H. Iwahara, T. Esaka, J. Appl. Electrochem. 7 (1977) 31.
[10] M.J. Verkerk, A.J. Burggraaf, J. Electrochem. Soc. 128 (1981) 75.
[11] T. Takahasi, H. Iwahara, T. Esaka, J. Electrochem. Soc. 124 (1977) 1563.
[12] T.E. Crumpton, J.F.W. Mosselmans, C. Greaves, J. Mater. Chem. 15 (2005) 164.
[13] T. Fries, G. Lang, S. Kemmler-Sach, Solid State Ionics 89 (1996) 233.
[14] N. Sharma, R.L. Withers, K.S. Knight, C.D. Ling, J. Solid State Chem. 182 (2009) 2468.
[15] B. Ravel, M. Newville, J. Synchrotron Radiat. 12 (2005) 537.
[16] I.D. Brown, D. Altermatt, Acta Crystallogr. B 41 (1985) 244.
[17] A.K. Cheetham, A.R. Rae-Smith, Acta Crystallogr. B 41 (1985) 225.
[18] H.A. Harwig, Z. Anorg. Chem. 444 (1978) 151.
[19] R. Punn, I. Gameson, F. Berry, C. Greaves, J. Phys. Chem. Solids 69 (2008) 2687.
[20] R. Punn, A.M. Feteria, D.C. Sinclair, C. Greaves, J. Am. Chem. Soc. 128 (2006) 15386.